

Exotic magnetization curves in classical square-kagomé spin lattices

Heinz-Jürgen Schmidt*

Fachbereich Mathematik/Informatik/Physik, Universität Osnabrück, 49069 Osnabrück, Germany.

Johannes Richter

*Institut für Physik, Universität Magdeburg, P.O. Box 4120, D-39016 Magdeburg, Germany and
Max-Planck-Institut für Physik Komplexer Systeme,
Nöthnitzer Straße 38, D-01187 Dresden, Germany*

Classical spin systems with non-coplanar ground states typically exhibit nonlinear magnetization curves characterized by kinks and jumps. Our article briefly summarizes the most important related analytical results. In a comprehensive case study, we then address AF-square kagomé and AF/FM-square kagomé spin lattices equipped with additional cross-plaquette interactions. It is known that these systems have non-coplanar ground states that assume a cuboctahedral structure in the absence of a magnetic field. When a magnetic field H is switched on, a rich variety of different phases develops from the cuboctahedral ground state, which are studied in their dependence on H and a cross-plaquette coupling constant $J_3 > 0$. For the AF square-kagomé spin lattice, we carefully identify and describe seven phases that appear in a phase diagram with five triple points. The transitions between these phases are predominantly discontinuous, although two cases exhibit continuous transitions. In contrast, the phase diagram of the AF/FM square-kagomé model shows only four phases with a single triple point, but these also lead to exotic magnetization curves. Here, too, there are two types of phase boundaries belonging to continuous and discontinuous transitions.

I. INTRODUCTION

Classical Heisenberg spin models with exclusively non-coplanar ground states are attractive for various reasons. These non-coplanar ground states break a chiral \mathbb{Z}_2 symmetry, leading to phase transitions at finite temperature, even in two space dimensions, while conventional magnetic order is, for the Heisenberg models of interest here, subject to the Mermin-Wagner theorem [1]. Another motif to study such systems is the possible route to arriving at quantum spin liquids via frustration-induced quantum melting of magnetic orders, see [2].

Examples of spin systems with non-coplanar ground states can be found in the recent literature. A non-coplanar ground state called *cuboc2* was found in Ref. [3] for the classical AF kagomé with ferromagnetic next-neighbor exchange J_1 and antiferromagnetic 2nd-neighbor exchange J_2 . The analogous *cuboc1* phase was first reported in Refs. [4, 5] for the classical AF kagomé with antiferromagnetic next-neighbor exchange J_1 and 3rd-neighbor exchange J_d along the diagonals of the hexagons. Later, these phases were systematically analyzed in Ref. [6], and the notations *cuboc1* and *cuboc2* were introduced to be explained in more detail in the next paragraph.

A similar spin system on a lattice with corner-sharing triangles is the square-kagomé Heisenberg antiferromagnet (SKHAF), that was introduced about 20 years ago [7–17]. Over the past five years, this system has attracted increasing attention in theoretical [18–27] as well as experimental [28–32] investigations.

A recent study [26] focuses on the SKHAF with longer-range Heisenberg couplings J_\times and J_+ across the octagonal plaquettes, see Fig. 1. The spin sites of the square-kagomé lattice can be divided into two non-equivalent classes, class A sites, which form the squares, and class B sites, which are in the middle of the bow ties connecting the squares, see Fig. 1. The couplings between the A spins in the squares are denoted by J_1 and the couplings between the A spins and the B spins by J_2 . For fully antiferromagnetic (AF) bonds, the spin vectors of the classical ground state form a *cuboctahedron*, one of the 13 Archimedean solids. This ground state shows angles of 120° between neighboring spin and is called a *cuboc1 state*. By inverting the sign of J_2 one obtains a variant of the square-kagomé lattice called AF/FM square-kagomé. Its ground state will be the so-called *cuboc3 state* obtained by flipping the B spins of the *cuboc1 state*.

In this work, we will continue the investigations of [26] by considering the ground states of the AF and AF/FM square-kagomé lattice in the presence of a magnetic field $(0, 0, H)$ giving rise to an additional Zeeman term in the Hamiltonian. Important characteristics to be studied are the magnetization curves $M(H)$ for different values of the coupling constants, S_i^z -plots of the z components of the ground state spins as a function of H , and the phase diagrams

*Electronic address: hschmidt@uos.de

showing different types of ground states as a function of H and the coupling constants. To keep the representation simple, we have largely restricted ourselves to the case of $J_1 = 1$, $J_2 = \pm 1$ and $J_x = J_y = J_z > 0$. We then have two phase diagrams corresponding to $J_2 = \pm 1$ in the $H - J_3$ plane.

The reason why we expect interesting magnetization curves for a spin system with a non-coplanar ground state is as follows. A classical spin system with a coplanar ground state with vanishing magnetization $M = 0$ at $H = 0$ always has a linear magnetization curve $M(H)$ with ground states approaching the fully aligned FM state, similar to the struts of an umbrella when it is folded. For a spin system with a non-coplanar ground state with $M = 0$ for $H = 0$, the analogous construction would also lead to a linear magnetization curve, but corresponding to a 4-dimensional and thus unphysical family of umbrella states. The necessity of a physical restriction to at most 3-dimensional ground states, on the other hand, leads to a non-linear magnetization curve that typically exhibits jumps and kinks.

In fact, such “exotic” magnetization curves have so far been described mainly for spin systems with non-coplanar ground states for $H = 0$, see [33–38]. Recently in Ref. [39] unconventional classical nonlinear magnetization curves have been found for a frustrated spinel and the J_1 - J_d AF kagomé.

The paper is organized as follows. In Section II we briefly describe the numerical, semi-analytical and analytical methods used in the paper. Section III is devoted to the study of the AF square-kagomé. We find seven phases, additional to the cuboc1 state for $H = 0$ and the FM phase for the saturation regime, that are described in Section III A together with typical magnetization curves and an S_i^z -plot for $J_3 = 0.1$. All phases are non-coplanar like the cuboc1 ground state for $H = 0$. There are discontinuous as well as continuous phase transitions. Phase IV, which is adjacent to the FM phase, can be described analytically by a parameter representation, as explained in the Appendix C. For $J_3 \lesssim 0.14$ there is a remarkable phase VII, different from the other ones, with a large, possibly macroscopic degeneracy.

The phase diagram for the AF/FM square-kagomé model is somewhat simpler, consisting only of four phases, see Section IV. Also here all phases are non-coplanar, except the analytical phase IV adjacent to the FM regime. Moreover, the magnetization curve in phase IV is linear, whereas all other parts of $M(H)$ are nonlinear.

The above-mentioned results are mainly obtained numerically or semi-analytically. In the section V and in the appendix B we present some analytical results for the area under the (normalized) magnetization curve (“sum rule”), which are valid for general Heisenberg spin systems. Some of these results are already known, but are scattered in the literature. For example, this area F is always equal to or larger than the area $\frac{1}{2}H_{\text{sat}}$ given by the linear magnetization curve. The latter case, i.e. $F > \frac{1}{2}H_{\text{sat}}$, which is typical for exotic magnetization curves, can be predicted by an analysis of the matrix of coupling constants. Related analytical results on the saturation field H_{sat} are contained in Appendix A. We close with a Summary and Outlook in Section VI.

II. METHODS

Let us briefly describe the used methods. Similar as in Ref. [26] we use a Monte-Carlo like approach to get numerical data for the energy E_0 , the magnetization M and spin-spin correlations $\mathbf{s}_i \cdot \mathbf{s}_j$ in the classical ground state.

We also use a semi-analytical approach introduced in [26], which works as follows: Starting from a ground state for a system of N classical spins \vec{s}_i , which we obtain numerically from our Monte Carlo calculation, we form groups of spin vectors pointing approximately in the same direction, i. e., satisfying, say, $\mathbf{s}_i \cdot \mathbf{s}_j \geq 0.995$. This gives a set of M distinct spin directions, which is further reduced by guessing their symmetry group. In the end, we have K different spin directions for the ground state, of which we obtain all others by applying symmetry operations. Next, we calculate the energy (including the Zeeman term) of the spin configuration $\mathcal{K}(\alpha_1, \dots, \alpha_n)$ as a function of some parameters $\alpha_1, \dots, \alpha_n$ describing the position of the remaining K spin vectors. This energy is minimized numerically, starting with the initial numerical values of the parameters corresponding to the K spin vectors. It should have become clear that the semi-analytical method cannot be applied schematically, but requires a certain intuition. Faulty identifications of closely neighboring spins usually show up in too high ground state energies. Conversely, a slight lowering of the initial numerical energy is an indication of a successful application of the method.

In special cases, typically in the last phase before saturation, it is possible to solve the system of equations $0 = \partial\mathcal{K}/\partial\alpha_i$, $i = 1, \dots, n$ analytically and thus obtain explicit or parametric expressions for the magnetization curve. Alternatively, we used a generalized Luttinger-Tisza method [40] to obtain analytical results for the latter case. This method provides rigorous results and it can be used to confirm the semi-analytical results.

III. AF SQUARE-KAGOMÉ

Like the kagomé lattice the square-kagomé consists of corner-sharing triangles, but enclosing squares instead of hexagons. Another difference to the kagomé lattice is the existence of two non-equivalent sites A (forming the squares)

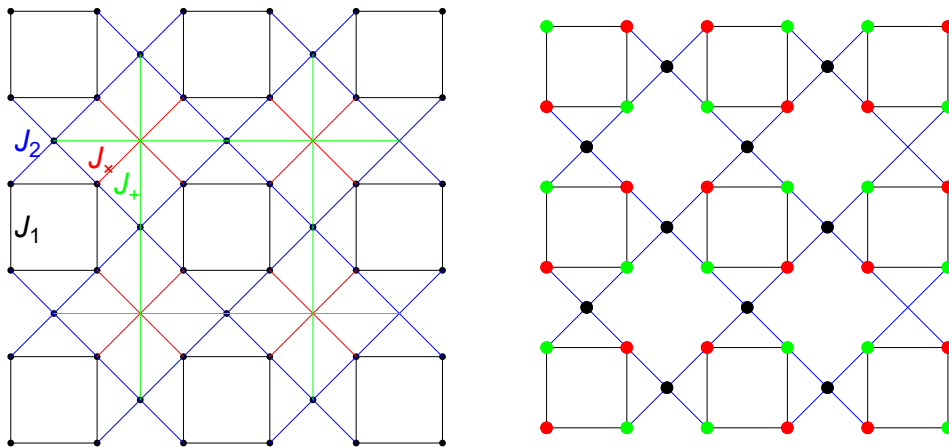


FIG. 1: Left panel: The square-kagomé J_1 - J_2 model with cross-plaquette interactions J_+ and J_x . We distinguish between sites A forming the squares (black lines) and sites B at the center of the bow ties (blue lines).

Right panel: Sketch of phase IV for the AF/FM square-kagomé lattice, see Section IV B 4. The black dots at sites B represent spin vectors of the form $\mathbf{s}_i = (0, 0, 1)$, and the red/green dots at sites A spin vectors of the form $\mathbf{s}_i = (\pm\sqrt{1-z_1^2}, 0, z_1)$, where z_1 is given below, see Eq. (5).

and B (center of the bow ties) as well as two non-equivalent nearest neighbor bonds J_1 and J_2 . The corresponding model is depicted in Fig. 1, left panel. For numerical and some analytical calculations we have to approximate the infinite square-kagomé lattice by a finite lattice model \mathcal{L} with periodic boundary conditions. We may view $\mathcal{L} = (\mathcal{V}, \mathcal{E})$ as an undirected graph with vertex set $\mathcal{V} = \{1, \dots, N\}$ representing the spin sites and a set of edges

$$\mathcal{E} = SQ \cup BT \cup C \cup \mathcal{P}, \quad (1)$$

representing, resp., the interacting pairs within the squares, bow ties, the diagonal cross-plaquette pairs, and the vertical/horizontal ones. Then the Hamiltonian \mathcal{H} (without Zeeman term) can be written as

$$\mathcal{H} = \sum_{(i,j) \in SQ} J_1 \mathbf{s}_i \cdot \mathbf{s}_j + \sum_{(i,j) \in BT} J_2 \mathbf{s}_i \cdot \mathbf{s}_j + \sum_{(i,j) \in C} J_x \mathbf{s}_i \cdot \mathbf{s}_j + \sum_{(i,j) \in \mathcal{P}} J_+ \mathbf{s}_i \cdot \mathbf{s}_j, \quad (2)$$

see Fig. 1, left panel.

Recall that the zero-field cuboc ground-state phase is present in the entire parameter region $J_+, J_x > 0$ independent of the magnitudes of J_+ and J_x , see Fig. 5 in Ref. [26]. For the sake of simplicity we therefore consider only the symmetric case $J_+ = J_x = J_3 > 0$ and further set $J_1 = J_2 = 1$.

A. Phase diagram

In the phase diagram (Fig. 2) we have chosen $0 \leq J_3 \leq 2$ and $0 \leq H \leq 10 + 2\sqrt{2} = 12.8284\dots$ according to the value of $H_{\text{sat}} = 4 + 3J_3 + \sqrt{4 + J_3^2}$, see (A7), for $J_3 = 2$. There are seven phases I - VII, additionally to the cuboc1 ground state for $H \rightarrow 0$ and the ferromagnetic ground state FM for $H \geq H_{\text{sat}}$. We obtain two continuous transitions (additional to the transition IV-FM), corresponding to the phase boundary between IV and VII and the phase boundary between II and III. In both cases of continuous transitions, we have a subgroup relationship between the symmetry groups of the phases involved, as it must necessarily be. The magnetization jump ΔM at the phase boundary between I and II varies over three decades and, for $J_3 \gtrsim 1.6$, is hardly visible in the numerically calculated magnetization curves. We observe five triple points $T_i, i = 1, \dots, 5$, where three phase boundaries intersect and three phases touch, see the cyan points in Fig. 2 and Table I. As a consequence there are six types of magnetization curves, see Table I and Fig. 3.

B. Description of single phases

Here we describe the seven phases of the phase diagram in Fig. 2. The corresponding ‘‘common-origin plots’’ in this Figure provide a graphical illustration of their spin structure. In a common-origin plot, the entire ground

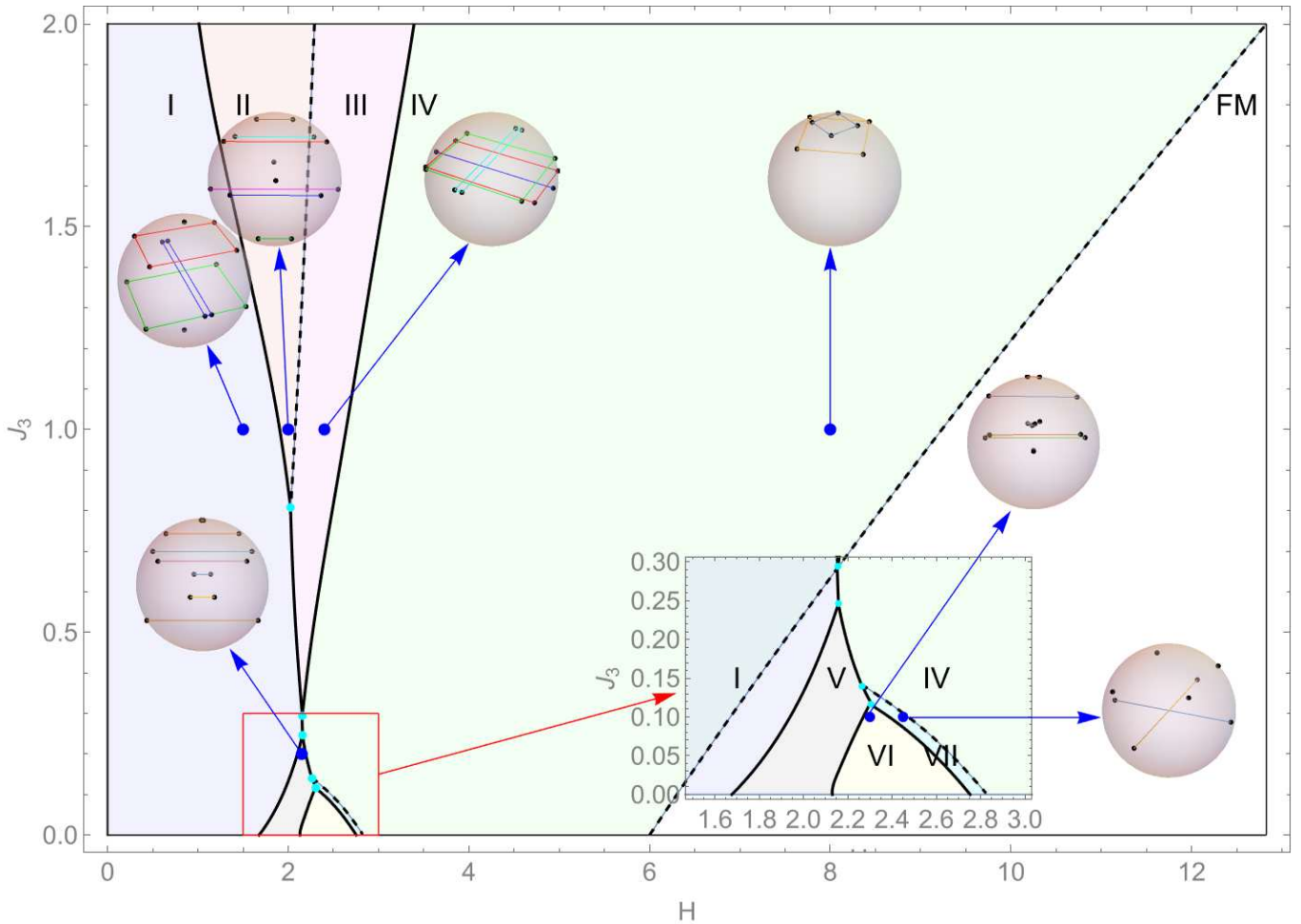


FIG. 2: Phase diagram for the AF square-kagomé model in the $H - J_3$ -plane, where H denotes the magnetic field and J_3 the additional cross-plaquette coupling. We have chosen $0 \leq J_3 \leq 2$ and $0 \leq H \leq 12.8284\dots$. There are seven phases I - VII, additional to the cuboc1 ground state for $H \rightarrow 0$ and the ferromagnetic ground state FM for $H \geq H_{\text{sat}}$ and five triple points (cyan color). The solid curves represent discontinuous phase transitions and the dashed lines continuous ones. For the region $1.5 \leq H \leq 3$ and $0 \leq J_3 \leq 0.3$ we have added an enlargement in the form of an inset. Typical common-origin plots for all seven phases have been inserted such that the corresponding point in the $H - J_3$ -plane is indicated by a blue dot.

state configuration of spins in real space is concentrated into a point cloud on a single unit sphere. We also show one representative example of the field dependence of the z -components of the spin vectors of the ground state configuration in Fig. 4.

1. Phase I

We observe 14 different spin vectors, two of which occupy the north and south pole of the unit sphere and the remaining 12 are distributed on three different circles with constant z in groups of four. These groups form rectangles with parallel edges. Hence the symmetry group of this phase is D_2 , the symmetry group of the rectangle. For $H \rightarrow 0$ the points of the center rectangle merge in pairs, and the resulting 12 spin vectors form a cuboctahedron. We show an example corresponding to $H = 1.5$ and $J_3 = 1$, see Fig. 2. In every finite model of the square-kagomé lattice with N spin sites, $N = 6L^2$, L even, 10 spins occupy sub-lattices with $N/12$ sites and four spins occupy sub-lattices with $N/24$ sites. The partial merging for $H \rightarrow 0$ results in the 12 sublattices of the cuboc1 state, each with $N/12$ sites.

TABLE I: Coordinates of the five triple points T_i , $i = 1, \dots, 5$ in the phase diagram (Fig. 2) and the type of magnetization curves for values of J_3 between the triple points. When listing the jumps and kinks in the magnetization curve we always neglect the kink at $H = H_{\text{sat}}$.

i	$H = h_i$	$J_3 = j_i$	interval	jumps (\mathcal{J}) and kinks (\mathcal{K})
1	2.02593	0.80768	$j_1 < J_3$	$\mathcal{J} \mathcal{K} \mathcal{J}$
2	2.1556	0.294157	$j_2 < J_3 < j_1$	$\mathcal{J} \mathcal{J}$
3	2.15822	0.246352	$j_3 < J_3 < j_2$	\mathcal{J}
4	2.26488	0.13962	$j_4 < J_3 < j_3$	$\mathcal{J} \mathcal{J}$
5	2.30494	0.116264	$j_5 < J_3 < j_4$	$\mathcal{J} \mathcal{J} \mathcal{K}$
			$0 < J_3 < j_5$	$\mathcal{J} \mathcal{J} \mathcal{J} \mathcal{K}$

2. Phase II

We observe 14 different spin vectors, which are pairwise distributed on six different circles with constant z and two further spin vectors with different z , see the example in Figure 2 for $H = 1.5$ and $J_3 = 1$. There is a reflection symmetry which can be described as $y \leftrightarrow -y$ upon a suitable choice of the coordinate system and hence the symmetry group is D_1 .

3. Phase III

If H is increased beyond a critical value, the eight circles of phase II merge into four circles with constant z_i , $i = 1, \dots, 4$, and thus form a continuous transition to another phase called III. Three of these circles contain rectangles with parallel edges formed by spin vectors and the fourth circle contains a pair of antipodal spin vectors, also parallel to the edges of the rectangles, see the example in Figure 2 for $H = 2.4$ and $J_3 = 1$. This spin configuration has thus D_2 -symmetry. Since z_1 and z_3 are very close to each other, the corresponding circles cannot be distinguished by eye.

4. Phase IV

Further increasing H (e. g. beyond $H = 2.8$ at $J_3 = 1.0$) we obtain a new phase denoted by IV. It consists of eight different spin vectors, which are distributed on two circles with constant $z = z_i$, $i = 1, 2$, see the example in Figure 2 for $H = 8$ and $J_3 = 1$. The two groups of spin vectors form two squares twisted by 45° . Hence this ground state has a D_4 symmetry.

This phase can be analytically described by a parameter representation. Relevant quantities as magnetic field, z_1 , z_2 , magnetization and energy can be expressed as functions of a parameter w that varies between 1 and $w_{\text{max}}(J_3)$. These functions are specified in Appendix C.

5. Phase V

For small values of J_3 , by increasing H we enter a new phase V directly from phase I (e. g. for $J_3 = 0.2$ at $H = 2.10188$), where phase V is similar to phase II. We observe 14 different spin vectors, which are pairwise distributed on seven different circles with constant z , see the example in Figure 2 for $H = 2.15$ and $J_3 = 0.2$. There is a D_1 reflection symmetry which can be described as $y \leftrightarrow -y$ upon a suitable choice of the coordinate system.

6. Phase VI

Below the triple point T_5 phase V gives way for a new phase IV (e. g. for $J_3 = 0.1$ at $H = 2.387$). We observe 14 different spin vectors, which are pairwise distributed on seven different circles with constant z forming pairs, see the example in Figure 2 for $H = 2.3$ and $J_3 = 0.1$. The symmetry of this phase is the rotation of the $x - y$ -plane with 180° , or $(x, y) \leftrightarrow (-x, -y)$ and hence its symmetry group of order 2 can be chosen as C_2 in order to distinguish it from the reflection symmetry group D_1 of phase II.

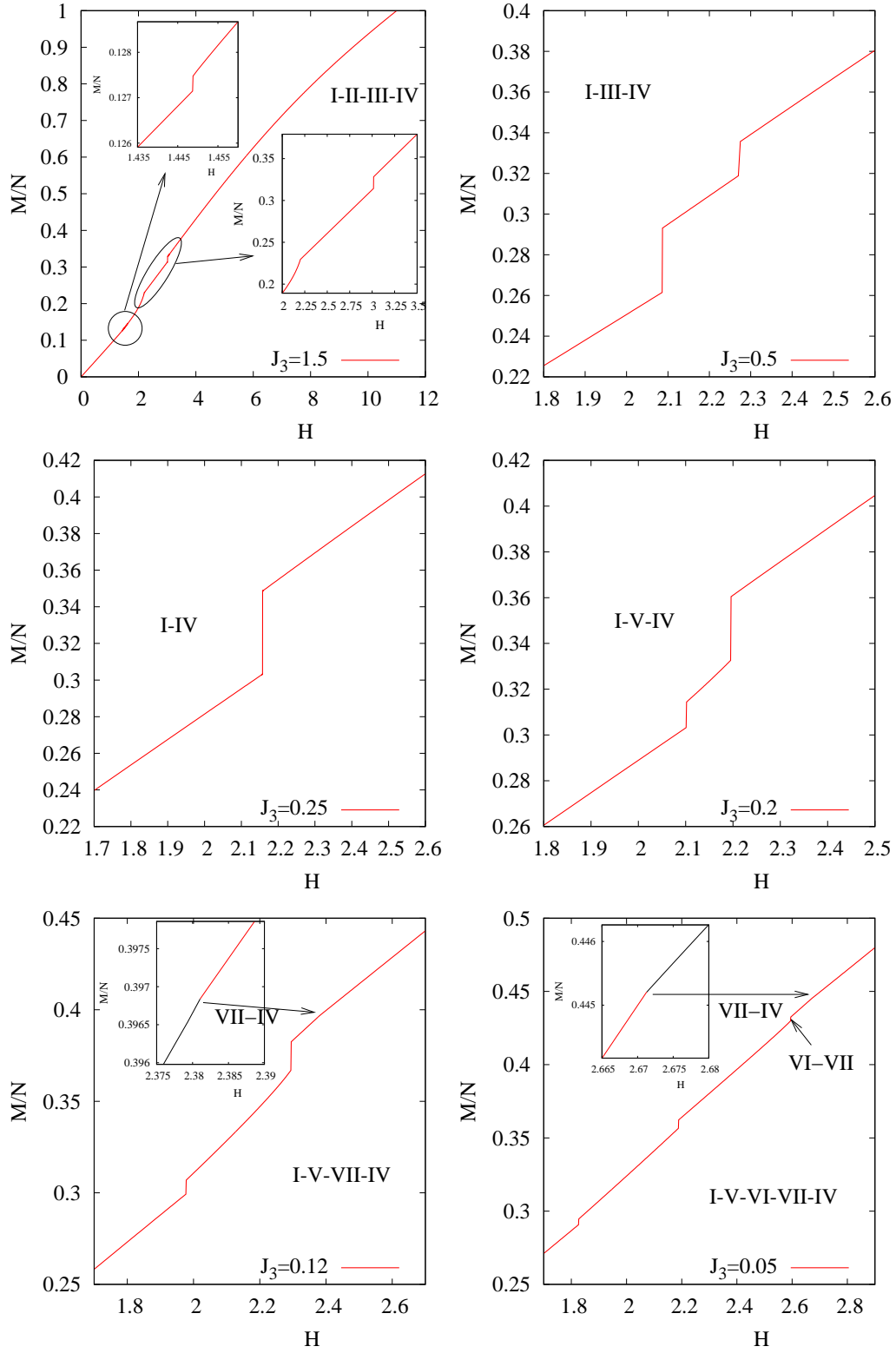


FIG. 3: According to Table I and the phase diagram in Figure 2 there are six different types of magnetization curves, of which we show typical sections that were calculated numerically. From top to bottom, J_3 assumes the values $J_3 = 1.5, 0.5, 0.25, 0.2, 0.12, 0.05$. In the cases where the magnetization jumps or kinks are not visible, we have inserted enlargements in the form of insets. The two insets for $J_3 = 0.12$ and $J_3 = 0.05$ are based on semi-analytical calculations.

7. Phase VII

For $J_3 = 0.1$ and $2.387 < H < 2.47456$ we obtain a new, disordered phase denoted by VII. It has a large degeneracy, as shown by Figure 4, reminiscent of the spin liquid for $J_3 = H = 0$, see [26]. For the semi-analytical calculation we have randomly picked out a variety of ground state configurations of this phase and found eight different spin vectors, such that four of them are arbitrarily positioned on the unit sphere and the remaining four spin vectors forming antipodal pairs, see the example in Figure 2 for $H = 2.45$ and $J_3 = 0.1$. The symmetry group of this phase is thus reduced to the identity. Both groups of spin vectors have strictly separated z -values. As H increases and approaches the phase boundary between phase VII and IV, the z values of the first group (with uncorrelated z -values) converge towards some value $z_I > 0$, while the z values of the second group (forming antipodal pairs) converge towards $z_{II} = 0$, see Figure 4. This numerical finding suggests the approach of analytically determining the phase boundary VII/IV by the condition that one of the two z -values in phase IV is equal to 0. The result

$$J_3 = 1 - \frac{2}{\sqrt{8 - \frac{H^2}{2}}} \quad (3)$$

agrees very well with the semi-analytically calculated phase boundary. It follows that the first, non-zero limit value for z is

$$z_I = \frac{\sqrt{(J_3 - 2)J_3 + \frac{1}{2}}}{1 - J_3}. \quad (4)$$

For $J_3 = 0.1$ used in Fig. 4 we have $z_I = 0.61864$. The corresponding phase transition is continuous.

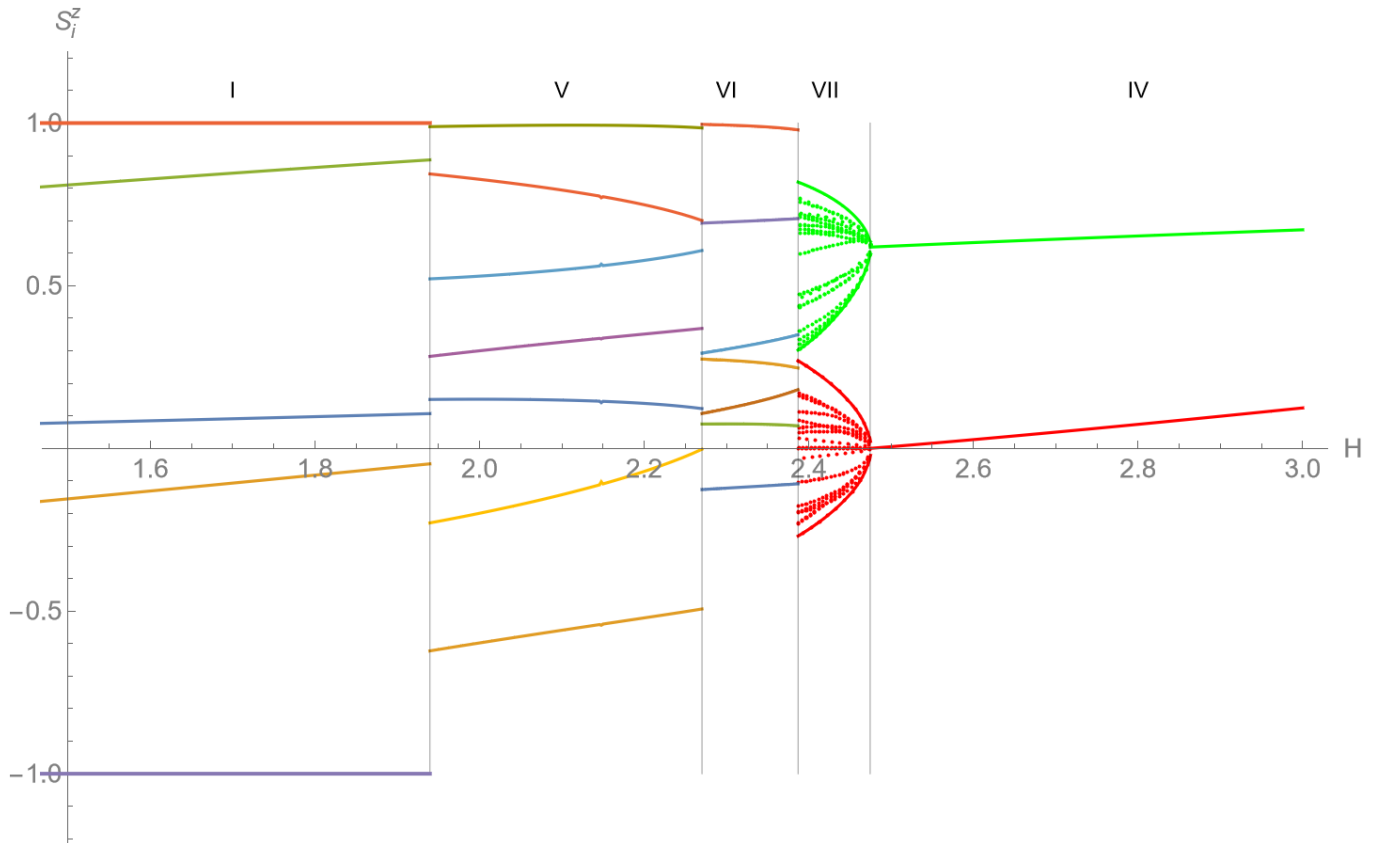


FIG. 4: The z -components of the spin vectors of the ground state configuration semi-analytically calculated for $J_1 = J_2 = 1$, $J_3 = 0.1$ and $1.5 \leq H \leq 3.0$. We can distinguish all five phases I,V,VI,VII,IV, similarly as in the magnetization curve, see Figure 3, lower right panel. Note the large degeneracy of the ground states of phase VII for $2.387 < H < 2.47456$, of which we have only drawn a selection.

IV. AF/FM SQUARE-KAGOMÉ

The AF/FM square-kagomé is obtained for $J_1 > 0$ and $J_2 < 0$, i. e. for AF couplings within the squares and FM couplings within the bow ties connecting the squares. If the magnetic field vanishes, the AF/FM case can be reduced to the AF case by simultaneously inverting the sign of J_2 and flipping the spin vectors at the sites B (sitting in the center of the bow ties), leaving the Hamiltonian unchanged. Consequently, the ground state in the quadrant $J_\times, J_+ > 0$ will be the cuboc3 spin configuration obtained from the cuboc1 ground state of the AF square-kagomé by flipping the spins at sites B, see [26]. However, the Zeeman term is not invariant under this transformation, so that the magnetization of the AF/FM square kagomé must be investigated separately. For this we set $J_1 = 1$ and $J_2 = -1$ and restrict ourselves to the diagonal $J_\times = J_+ =: J_3 > 0$.

A. Phase diagram

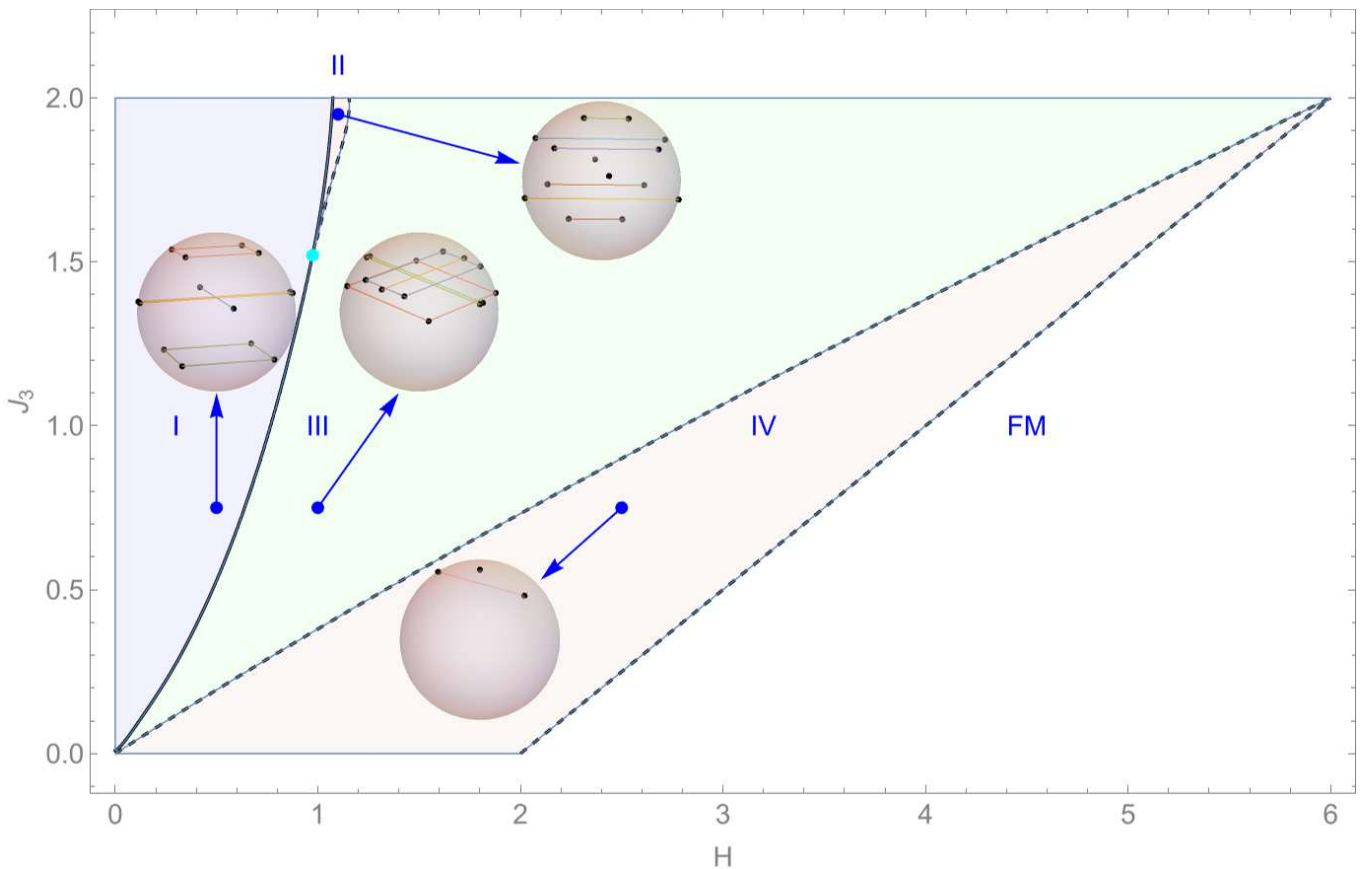


FIG. 5: Phase diagram for the AF/FM square-kagomé model in the $H - J_3$ -plane, where H denotes the magnetic field and J_3 the additional cross-plaquette coupling. We have chosen $0 \leq J_3 \leq 2$ and $0 \leq H \leq 6$. In addition to the cuboc3 ground state for $H \rightarrow 0$ and the ferromagnetic ground state FM for $H \geq H_{\text{sat}}$ there are four phases I - IV and one triple point (cyan color). The solid curves represent discontinuous phase transitions and the dashed ones continuous phase transitions.

In the phase diagram, see Fig. 5, we have chosen $0 \leq J_3 \leq 2$ and $0 \leq H \leq 6$ according to the value of $H_{\text{sat}} = 2(1+J_3)$, see (A9), for $J_3 = 2$. There are four phases I - IV, additionally to the cuboc3 ground state for $H \rightarrow 0$ and the ferromagnetic ground state FM for $H \geq H_{\text{sat}}$. We found two continuous transitions (additional to the transition IV - FM) corresponding to the phase boundaries between II and III and between III and IV. In both cases there is a symmetry group inclusion of the form $D_1 \subset D_2$. We obtain one triple point at $H = h_1 = 0.974276$, $J_3 = j_1 = 1.52014$, where the three phases I,II, III touch, see the cyan point in Fig. 5. As a consequence there are two types of magnetization curves, one with one jump and one kink for $J_3 > j_1$ and one with one jump and two kinks for $J_3 < j_1$, see Fig. 6. Two typical plots of the z -components of all ground state spin vectors depending on H are shown in Fig. 7.

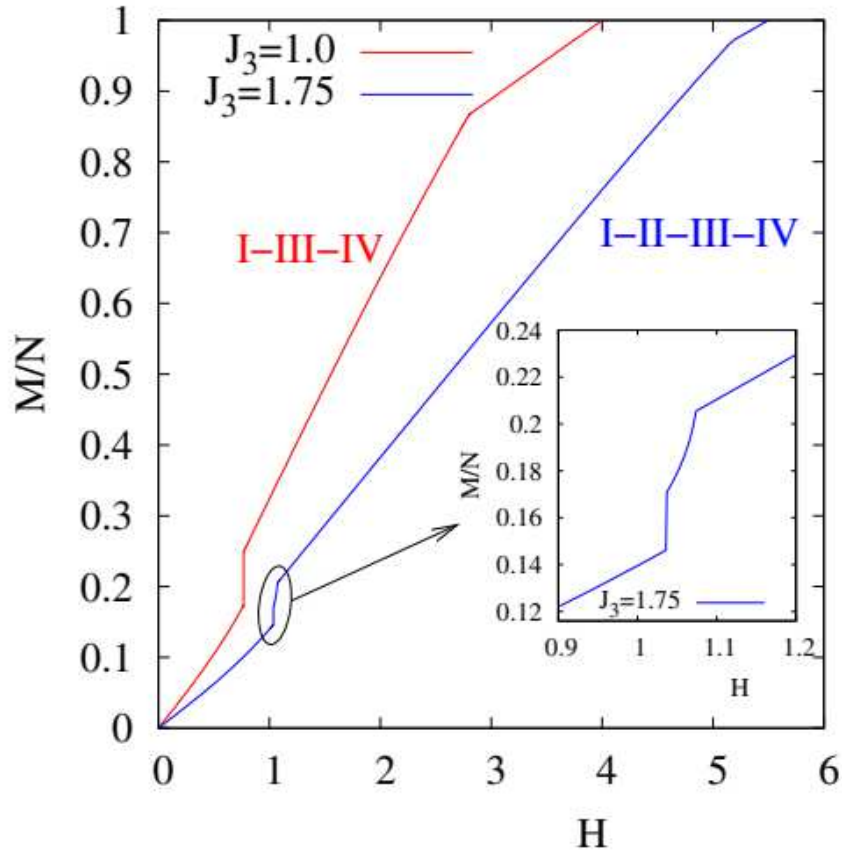


FIG. 6: According to the phase diagram in Figure 5, there are two different types of magnetization curves. We show typical $M(H)$ curves for the values $J_3 = 1.0$ and $J_3 = 1.75$ that were calculated numerically. In the case $J_3 = 1.75$ we have added an enlargement in the form of an inset to make the jump and the kink in the magnetization curve more clearly visible.

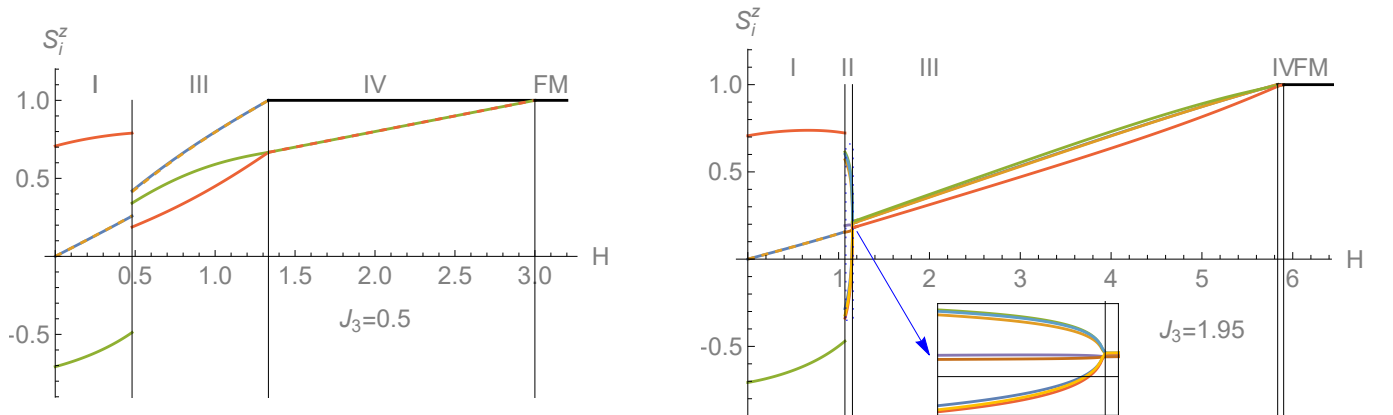


FIG. 7: The z -components of the spin vectors of the ground state configuration semi-analytically calculated for $J_1 = -J_2 = 1$, $0 \leq H \leq H_{\text{sat}}$, and two different values of J_3 .
 Left panel: $J_3 = 0.5$. We can distinguish the phases I-III-IV, similarly as in the left magnetization curve of Fig. 6.
 Right panel: $J_3 = 1.95$. Here also the phase II is visible and the continuous transition to phase III, see the enlargement in the inset.

B. Description of single phases

Here we describe the four phases of the phase diagram in Figure 5. The corresponding common-origin plots in this Figure provide a graphical illustration of their spin structure.

1. Phase I

For small H we observe a ground state configuration, called phase I, consisting of 14 spin vectors with four different z values z_i , $i = 1, \dots, 4$. They form three rectangles with parallel edges that can be chosen parallel to the x - and y -axis and a pair of the form $(\pm\sqrt{1-z_4^2}, 0, z_4)$. The symmetry group of phase I is hence D_2 . For $H \rightarrow 0$, one of the rectangles degenerates into a pair of spin vectors and the resulting 12 vectors form the cuboc3 ground state mentioned above.

2. Phase III

This phase is adjacent to phase I below the triple point, i. e., when $J_3 < j_1 = 1.52014$ and has the same structure as phase I, i. e., consisting of three rectangles and one pair, also with the symmetry group D_2 , but a different energy. When approaching the boundary to phase IV, see below, one of the rectangles and the pair of spin vectors converge towards the north pole $(0, 0, 1)$ of the unit sphere and the other two rectangles approach two vectors of the form $(\pm\sqrt{1-z_1^2}, 0, z_1)$, resulting in a continuous transition to phase IV.

3. Phase II

Above the triple point, i. e., when $J_3 > j_1 = 1.52014$, there exists another phase, called phase II, located between phase I and phase III. It consists of 14 spin vectors forming six pairs related by the symmetry $y \leftrightarrow -y$, if we choose the coordinated system correspondingly, and two further spin vectors with $y = 0$. The symmetry group is thus D_1 .

4. Phase IV

This phase is the only one with coplanar spin structure and consequently the corresponding part of the magnetization curve is linear. It can be analytically described and consists of three different sublattices of spin vectors of the form $\mathbf{s}_i = (0, 0, 1)$ and $\mathbf{s}_i = (\pm\sqrt{1-z_1^2}, 0, z_1)$ distributed on the spin lattice according to Fig. 1, right panel. Hence phase IV has thus the same symmetry group D_1 as phase II. The various quantities as z_1 , magnetization M/N and energy E are given as functions of H and J_3 by

$$z_1 = \frac{H+2}{2(J_3+2)}, \quad (5)$$

$$M/N = \frac{H+J_3+4}{3(J_3+2)}, \quad (6)$$

$$E = \frac{(H+2)(H+2J_3+6)}{6(J_3+2)}. \quad (7)$$

For $H \rightarrow H_{\text{sat}} = 2(1+J_3)$ it follows that $z_1 \rightarrow 1$ and $M/N \rightarrow 1$, i. e., the ground state approaches the FM state.

V. SUM RULE FOR MAGNETIZATION CURVES

In this section we will formulate some results on the area below the magnetization curves for the square-kagomé systems that we consider in this article and which are of relevance for the exotic character of these curves. More general results that hold for general classical Heisenberg spin systems are proven in Appendix B.

For a linear magnetization curve $M/N = \frac{H}{H_{\text{sat}}}$ (dotted line in Figure 8) the area F below the graph of M/N is $\frac{1}{2}H_{\text{sat}}$. In general, one can show that $F \geq \frac{1}{2}H_{\text{sat}}$, see Appendix B. Hence $F > \frac{1}{2}H_{\text{sat}}$ implies that the magnetization curve cannot be completely linear and may show exotic features as jumps or kinks.

For the AF square-kagomé with $J_1 = J_2 = 1$ and $J_+ = J_- =: J_3$ we have the following result:

$$\Delta F := F - \frac{1}{2} H_{\text{sat}} = -1 + \frac{1}{2} \sqrt{J_3^2 + 4} + \frac{J_3}{6} > 0, \quad (8)$$

for all $J_3 > 0$ thus indicating exotic magnetization curves. To give a numerical example: For $J_3 = 1$, corresponding to Figure 8, we have $H_{\text{sat}} = 12.8284$ and the numerical integration of the magnetization curve yields $\Delta F = 0.2847003$, very close to the analytical value of $\Delta F = \frac{1}{6} (3\sqrt{5} - 5) = 0.2847006554\dots$

For AF/FM square-kagomé systems with $J_1 = -J_2 = 1$ and $0 \leq J_+ = J_- =: J_3 < 2$ the analogous result reads:

$$\Delta F := F - \frac{1}{2} H_{\text{sat}} = \frac{1}{2} (2 - J_3) > 0, \quad (9)$$

To give an example: For $J_3 = 1/2$ we have $H_{\text{sat}} = 3$ according to $H_{\text{sat}} = 2(1 + J_3)$, see (A9). The numerical integration of the magnetization curve yields $\Delta F = 0.50002$, very close to the analytical value of $\Delta F = 1/2$.

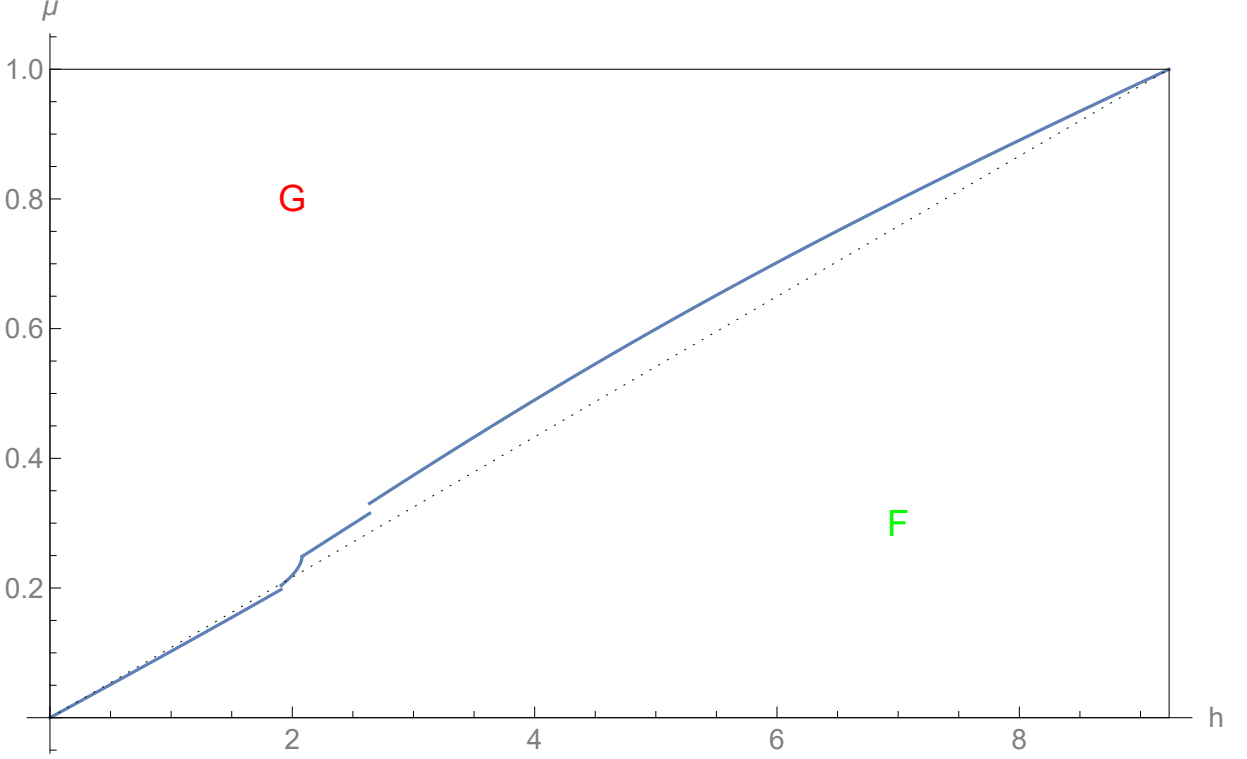


FIG. 8: Magnetization curve for the AF square-kagomé and coupling constants $J_1 = J_2 = J_3 = 1$, the area F below the magnetization curve and the complementary area G . The area $F \approx 4.90273$ is larger than the area $\frac{1}{2} H_{\text{sat}} \approx 4.618$ below the linear magnetization curve (dotted line).

VI. SUMMARY AND OUTLOOK

Spin systems with non-coplanar ground states are expected to have non-linear magnetization curves with kinks and jumps. In general, magnetization curves can only be studied numerically or semi-analytically, but some features can be determined analytically, e.g. the saturation field, the area under the magnetization curve and sometimes the last part of the curve just before saturation. We have compiled the corresponding analytical results in this paper.

As an extended case study, we have further investigated the AF square-kagomé and AF/FM square-kagomé lattices which are known to have exclusive non-coplanar ground states with cuboctahedral structure when the magnetic field vanishes. Indeed we found a diverse spectrum of ground state phases depending on the magnetic field H and a certain coupling constant $J_3 > 0$. The latter describes the strength of the additional cross-plaquette interactions.

For the AF square-kagomé, we were able to identify seven phases with five triple points and describe their structure in detail. The transitions between these phases are mostly discontinuous, but in two cases also continuous. They can

be characterized more precisely with so-called S_i^z -plots showing the z -components of all ground state spin vectors as a function of H . In contrast, the AF/FM square kagome has only four phases with one triple point, but also shows exotic magnetization curves with continuous as well as discontinuous phase transitions.

The question can be raised whether our results are typical for spin systems with cuboc ground states. As mentioned in the Introduction, cuboc phases were originally found in variants of the AF kagomé lattice. Therefore, the investigation of magnetization curves etc. for these models would be an obvious extension of the present work. Corresponding studies are in preparation.

Acknowledgment

We thank Martin Gembé, Ciarán Hickey, Yasir Iqbal and Simon Trebst for instructive discussions in connection with a common project on the square-kagomé spin lattices, from which the topic of the present paper developed.

Appendix A: Saturation fields

When the magnetic field H reaches or exceeds a certain saturation value H_{sat} , all spins align parallel to the direction of the magnetic field. In calculating H_{sat} for the systems considered in this work we have followed the approach presented in [40–42], which will be briefly recapitulated here. This approach is limited to finite spin systems but it turns out that the results for H_{sat} are independent of the system size (provided N is not too small) and hence also hold for the infinite square-kagomé spin lattice.

Thus we consider the matrix \mathbb{J} of coupling constants J_{ij} (with vanishing diagonal entries) and introduce the *dressed coupling matrix* $\mathbb{J}(\boldsymbol{\lambda})$ defined by

$$\mathbb{J}(\boldsymbol{\lambda})_{ij} := J_{ij} + \lambda_i \delta_{ij} \quad \text{for } i, j = 1, \dots, N, \quad (\text{A1})$$

with variable diagonal entries λ_i subject to the condition $\sum_i \lambda_i = 0$. The choice of $\boldsymbol{\lambda}$ will be often referred to as a *gauge*. The energy of the spin configuration is independent of the gauge. The minimal eigenvalue of $\mathbb{J}(\boldsymbol{\lambda})$ will be denoted by $j_{\min}(\boldsymbol{\lambda})$ and the absolute ground state energy is given by

$$E_{\min}/N = j_{\min}(\widehat{\boldsymbol{\lambda}}), \quad (\text{A2})$$

where $\widehat{\boldsymbol{\lambda}}$ is the *ground state gauge*. Another useful gauge is the *homogeneous gauge* $\widetilde{\boldsymbol{\lambda}}$ defined as follows. Consider the mean row sum of the undressed J -matrix \mathbb{J}

$$\tilde{j} := \frac{1}{N} \sum_{ij} J_{ij}, \quad (\text{A3})$$

and define

$$\widetilde{\lambda}_i := \tilde{j} - \sum_j J_{ij} \quad \text{for } i = 1, \dots, N. \quad (\text{A4})$$

It follows that \tilde{j} will be an eigenvalue of $\mathbb{J}(\widetilde{\boldsymbol{\lambda}})$ corresponding to the eigenvector $(1, 1, \dots, 1)$ representing a fully aligned spin configuration.

Then the saturation field is given by

$$H_{\text{sat}} = 2 \left(\tilde{j} - j_{\min}(\widetilde{\boldsymbol{\lambda}}) \right), \quad (\text{A5})$$

see [42]. Especially, if $\tilde{j} = j_{\min}(\widetilde{\boldsymbol{\lambda}})$ and hence $H_{\text{sat}} = 0$ the spin system will assume the ferromagnetic ground state $\uparrow \uparrow \dots \uparrow$ even for vanishing fields and hence has been called “ferromagnetic” in [42].

As an example we consider the AF square-kagomé with $J_1 = J_2 = 1$ and $J_\times, J_+ \geq 0$. It can be shown that

$$H_{\text{sat}} = \begin{cases} 2(3 + J_\times) & : J_\times \geq 2J_+, \\ 4 + J_\times + 2J_+ + \sqrt{(J_\times - 2J_+)^2 + 4} & : J_\times \leq 2J_+, \end{cases} \quad (\text{A6})$$

For the special case $J_+ = J_\times =: J_3 \geq 0$ considered in this paper this equation specializes to

$$H_{\text{sat}} = 4 + 3J_3 + \sqrt{4 + J_3^2}. \quad (\text{A7})$$

The analogous result for the AF/FM square-kagomé with $J_1 = -J_2 = 1$ and $J_+, J_\times \geq 0$ reads

$$H_{\text{sat}} = \begin{cases} 2(1 + J_\times) & : J_\times \geq 2J_+ - 2, \\ J_\times + 2J_+ - 2 + \sqrt{(J_\times - 2J_+ + 2)^2 + 4} & : J_\times \leq 2J_+ - 2, \end{cases} \quad (\text{A8})$$

For the special case $0 \leq J_+ = J_\times =: J_3 \leq 2$ considered in the examples in this paper this equation specializes to

$$H_{\text{sat}} = 2(1 + J_3) . \quad (\text{A9})$$

Appendix B: Sum rule for the magnetization curve of general Heisenberg spin systems

In this section we will formulate and prove some generalization of the results in Section V for general classical Heisenberg spin systems. Some of these results already appear in [42]. The notation to be introduced only applies to this section. Analogous results apply to quantum spin systems, but here the magnetization curve is a step function and its area can be expressed as a sum. This explains the wording ‘‘sum rule’’.

We consider the magnetization per site $\mu = M/N$ as a function $\mu(h)$ of the magnetic field h for $0 \leq h \leq h_{\text{sat}}$ and its inverse function by $h(\mu)$. The minimal energy per site (without Zeeman term) for given μ will be denoted by $\epsilon(\mu) := E_{\text{min}}(M)/N$. It follows that

$$h(\mu) = \frac{\partial \epsilon(\mu)}{\partial \mu} . \quad (\text{B1})$$

The total energy per site (with Zeeman term) will be denoted by

$$\mathbf{H}(h) := \epsilon(\mu(h)) - \mu(h) h . \quad (\text{B2})$$

Hence $\mathbf{H}(h)$ is the Legendre transform of $\epsilon(\mu)$, see [42], and

$$\frac{\partial \mathbf{H}(h)}{\partial h} = -\mu(h) . \quad (\text{B3})$$

Cum grano salis, this also applies if $\mu(h)$ is not differentiable for a finite number of points, as in the examples of exotic magnetization curves considered in this paper, see Figure 8.

The area F below the graph of $\mu(h)$ is given by

$$F = \int_0^{h_{\text{sat}}} \mu(h) dh \stackrel{(\text{B3})}{=} - \int_0^{h_{\text{sat}}} \frac{\partial \mathbf{H}(h)}{\partial h} dh = \mathbf{H}(0) - \mathbf{H}(h_{\text{sat}}) \quad (\text{B4})$$

$$= \epsilon(\mu(0)) - \epsilon(\mu(h_{\text{sat}})) + \mu(h_{\text{sat}}) h_{\text{sat}} = \epsilon(\mu(0)) - \epsilon(1) + h_{\text{sat}} , \quad (\text{B5})$$

since $\mu(h_{\text{sat}}) = 1$. The complementary area G above the graph of $\mu(h)$, see Figure 8, is given by

$$G := \int_{\mu(0)}^1 h(\mu) d\mu = h_{\text{sat}} - F = -\epsilon(\mu(0)) + \epsilon(1) . \quad (\text{B6})$$

Recall the definitions and results given in Appendix A. Then the absolute ground state energy is given by

$$\epsilon(\mu(0)) = j_{\text{min}}(\widehat{\boldsymbol{\lambda}}) , \quad (\text{B7})$$

where $\widehat{\boldsymbol{\lambda}}$ is the ground state gauge. Moreover, for the fully aligned FM state we obtain

$$\epsilon(1) = \frac{1}{N} \sum_{ij} J_{ij} = \tilde{j} , \quad (\text{B8})$$

the mean row sum of the undressed J -matrix. Recall that the saturation field is given by

$$h_{\text{sat}} = 2 \left(\tilde{j} - j_{\text{min}}(\widetilde{\boldsymbol{\lambda}}) \right) , \quad (\text{B9})$$

see (B9). This entails

$$F \stackrel{(B5)}{=} \epsilon(\mu(0)) - \epsilon(1) + h_{\text{sat}} \stackrel{(B7,B8,B9)}{=} j_{\min}(\widehat{\boldsymbol{\lambda}}) - \tilde{j} + 2 \left(\tilde{j} - j_{\min}(\widetilde{\boldsymbol{\lambda}}) \right) \quad (\text{B10})$$

$$= \frac{1}{2} h_{\text{sat}} + \left(j_{\min}(\widehat{\boldsymbol{\lambda}}) - j_{\min}(\widetilde{\boldsymbol{\lambda}}) \right). \quad (\text{B11})$$

In the case $j_{\min}(\widehat{\boldsymbol{\lambda}}) = j_{\min}(\widetilde{\boldsymbol{\lambda}})$ it follows that $F = G = \frac{1}{2} h_{\text{sat}}$. Especially this holds in the ‘‘parabolic’’ case where $\mu(h)$ is linear, i. e., $\mu(h) = \frac{h}{h_{\text{sat}}}$ (dotted line in Figure 8). In general, we have $F \geq \frac{1}{2} h_{\text{sat}}$, since $j_{\min}(\widehat{\boldsymbol{\lambda}}) \geq j_{\min}(\widetilde{\boldsymbol{\lambda}})$, see [41]. The condition $j_{\min}(\widehat{\boldsymbol{\lambda}}) > j_{\min}(\widetilde{\boldsymbol{\lambda}})$, or, equivalently, $F > \frac{1}{2} h_{\text{sat}}$ is hence an indication for an exotic magnetization curve, but, strictly speaking, it is neither necessary nor sufficient.

1. Sum rule for the AF square-kagomé

In order to apply this to the AF square-kagomé with $J_1 = J_2 = 1$ and $J_{\times}, J_+ \geq 0$ we have to make a case distinction.

a. Case of $J_{\times} < 2J_+$

We have the following results:

$$j_{\min}(\widehat{\boldsymbol{\lambda}}) = -1 - \frac{1}{3}(J_{\times} + J_+), \quad (\text{B12})$$

$$j_{\min}(\widetilde{\boldsymbol{\lambda}}) = \frac{1}{6} \left(-3\sqrt{(2J_+ - J_{\times})^2 + 4} - 4J_+ - J_{\times} \right), \quad (\text{B13})$$

$$\Delta F := F - \frac{1}{2} h_{\text{sat}} = -1 + \frac{1}{2} \sqrt{(2J_+ - J_{\times})^2 + 4} + \frac{1}{6} (2J_+ - J_{\times}) > 0, \quad (\text{B14})$$

thus indicating exotic magnetization curves for all $J_{\times} < 2J_+$. (B12) follows from eq. (9) in Ref. [26] and (B7).

b. Case of $J_{\times} \geq 2J_+$

We have the following results:

$$j_{\min}(\widehat{\boldsymbol{\lambda}}) = -1 - \frac{1}{3}(J_{\times} + J_+), \quad (\text{B15})$$

$$j_{\min}(\widetilde{\boldsymbol{\lambda}}) = -1 + \frac{1}{3}(J_+ - 2J_{\times}), \quad (\text{B16})$$

$$\Delta F := F - \frac{1}{2} h_{\text{sat}} = \frac{1}{3}(J_{\times} - 2J_+) \geq 0, \quad (\text{B17})$$

thus indicating exotic magnetization curves for all $J_{\times} > 2J_+$.

2. Sum rule for the AF/FM square-kagomé

To state the analogous results for the AF/FM square-kagomé with $J_1 = -J_2 = 1$ and $J_{\times}, J_+ \geq 0$ we make the following case distinction.

a. Case of $J_{\times} > 2J_{+} - 2$

We have the following results:

$$j_{\min}(\widehat{\boldsymbol{\lambda}}) = -1 - \frac{1}{3}(J_{\times} + J_{+}), \quad (\text{B18})$$

$$j_{\min}(\widetilde{\boldsymbol{\lambda}}) = \frac{1}{3}(-5 - 2J_{\times} + J_{+}), \quad (\text{B19})$$

$$\Delta F := F - \frac{1}{2}h_{\text{sat}} = \frac{1}{3}(J_{\times} - 2J_{+} + 2) > 0, \quad (\text{B20})$$

thus indicating exotic magnetization curves for all $J_{\times} > 2J_{+} - 2$. (B18) is identical to (B12) due to the fact that the AF and the AF/FM square-kagomé have the same ground state energy (without Zeeman term).

b. Case of $J_{\times} \leq 2J_{+} - 2$

We have the following results:

$$j_{\min}(\widehat{\boldsymbol{\lambda}}) = -1 - \frac{1}{3}(J_{\times} + J_{+}), \quad (\text{B21})$$

$$j_{\min}(\widetilde{\boldsymbol{\lambda}}) = \frac{1}{6} \left(-3\sqrt{(-J_{\times} + 2J_{+} - 2)^2 + 4} - J_{\times} - 4J_{+} + 2 \right), \quad (\text{B22})$$

$$\Delta F := F - \frac{1}{2}h_{\text{sat}} = \frac{1}{6} \left(3\sqrt{(J_{\times} - 2J_{+} + 2)^2 + 4} - J_{\times} + 2J_{+} - 8 \right) \geq 0, \quad (\text{B23})$$

thus indicating exotic magnetization curves for all $J_{\times} < 2J_{+} - 2$.

Appendix C: AF square-kagomé phase IV

It is possible to describe phase IV analytically for all values of $J_3 > 0$ if we assume that the ground state has the form described in the main text depending on two z -values z_1 and z_2 . Its energy $E(J_3, H, z_1, z_2)$ is given by

$$E(J_3, H, z_1, z_2) = \frac{1}{3} \left(-H(z_1 + 2z_2) + 2J_3(z_1^2 + z_2^2 - 1) + 2z_2^2 + 4z_1z_2 - 2\sqrt{2 - 2z_1^2}\sqrt{1 - z_2^2} \right). \quad (\text{C1})$$

Ground states of this phase satisfy $\partial E/\partial z_1 = \partial E/\partial z_2 = 0$. These equations admit a parametric solution of the following form:

$$z_1 = \frac{w(\sqrt{2}(J_3 - 1) + w)}{\sqrt{2}(2J_3 - 1)w + 2} W \quad (\text{C2})$$

$$z_2 = W \quad (\text{C3})$$

$$M = \frac{\sqrt{2}(5J_3 - 3)w + w^2 + 4}{3\sqrt{2}(2J_3 - 1)w + 6} W \quad (\text{C4})$$

$$H = \frac{2(\sqrt{2}J_3w^2 + (2J_3(J_3 + 1) - 1)w + \sqrt{2}(J_3 + 1))}{(2J_3 - 1)w + \sqrt{2}} W, \text{ where} \quad (\text{C5})$$

$$W := \frac{\sqrt{(w^2 - 1)((2J_3 - 1)w((2J_3 - 1)w + 2\sqrt{2}) + 2)}}{w\sqrt{\frac{1}{2}(8(J_3 - 1)J_3 + 1)w^2 + \sqrt{2}(3J_3 - 1)w - (J_3 - 2)J_3 + 1}}, \quad (\text{C6})$$

and w is a parameter satisfying $1 \leq w \leq w_{\max}(J_3)$. For example, $w_{\max}(J_3 = 1) = \frac{1+\sqrt{5}}{\sqrt{2}} = 2.28825\dots$

[1] N. D. Mermin and H. Wagner, "Absence of ferromagnetism or antiferromagnetism in one-or two-dimensional isotropic Heisenberg models," *Phys. Rev. Lett.*, vol. 17, no. 22, p. 1133, 1966. [Online]. Available: <https://journals.aps.org/prl/abstract/10.1103/PhysRevLett.17.1133>

- [2] C. Hickey, L. Cincio, Z. Papić, and A. Paramekanti, “Emergence of chiral spin liquids via quantum melting of noncoplanar magnetic orders,” *Phys. Rev. B*, vol. 96, p. 115115, 2017. [Online]. Available: <https://journals.aps.org/prb/abstract/10.1103/PhysRevB.96.115115>
- [3] J.-C. Domenge, P. Sindzingre, C. Lhuillier, and L. Pierre, “Twelve sublattice ordered phase in the $J_1 - J_2$ model on the kagomé lattice,” *Phys. Rev. B*, vol. 72, p. 024433, Jul 2005. [Online]. Available: <https://link.aps.org/doi/10.1103/PhysRevB.72.024433>
- [4] O. Janson, J. Richter, and H. Rosner, “Modified kagome physics in the natural spin-1/2 kagome lattice systems: Kapellasite $Cu_3Zn(OH)_6Cl_2$ and Haydeite $Cu_3Mg(OH)_6Cl_2$,” *Phys. Rev. Lett.*, vol. 101, no. 10, p. 106403, 2008. [Online]. Available: <https://journals.aps.org/prl/abstract/10.1103/PhysRevLett.101.106403>
- [5] —, “Intrinsic peculiarities of real material realizations of a spin-1/2 kagomé lattice,” in *J. Phys.: Conf. Ser.*, vol. 145, no. 1. IOP Publishing, 2009, p. 012008. [Online]. Available: <https://iopscience.iop.org/article/10.1088/1742-6596/145/1/012008/meta>
- [6] L. Messio, C. Lhuillier, and G. Misguich, “Lattice symmetries and regular magnetic orders in classical frustrated antiferromagnets,” *Phys. Rev. B*, vol. 83, p. 184401, May 2011. [Online]. Available: <https://link.aps.org/doi/10.1103/PhysRevB.83.184401>
- [7] R. Siddharthan and A. Georges, “Square kagome quantum antiferromagnet and the eight-vertex model,” *Phys. Rev. B*, vol. 65, p. 014417, Dec 2001. [Online]. Available: <https://link.aps.org/doi/10.1103/PhysRevB.65.014417>
- [8] J. Schnack, H.-J. Schmidt, J. Richter, and J. Schulenburg, “Independent magnon states on magnetic polytopes,” *Eur. Phys. J. B*, vol. 24, no. 4, pp. 475–481, 2001. [Online]. Available: <https://link.springer.com/article/10.1007/s10051-001-8701-6>
- [9] P. Tomczak and J. Richter, “Specific heat of the spin-1/2 Heisenberg antiferromagnet on squagome lattice,” *J. Phys. A: Math. Gen.*, vol. 36, no. 20, p. 5399, 2003. [Online]. Available: <https://doi.org/10.1088/0305-4470/36/20/304>
- [10] J. Richter, O. Derzhko, and J. Schulenburg, “Magnetic-field induced spin-peierls instability in strongly frustrated quantum spin lattices,” *Phys. Rev. Lett.*, vol. 93, p. 107206, Sep 2004. [Online]. Available: <https://link.aps.org/doi/10.1103/PhysRevLett.93.107206>
- [11] J. Richter, J. Schulenburg, P. Tomczak, and D. Schmalfuß, “The Heisenberg antiferromagnet on the square-kagome lattice,” *Cond. Matter Phys.*, vol. 12, no. 3, pp. 507–517, 2009. [Online]. Available: <https://doi.org/10.5488/CMP.12.3.507>
- [12] H. Nakano and T. Sakai, “The two-dimensional $s = 1/2$ Heisenberg antiferromagnet on the shuriken lattice – a lattice composed of vertex-sharing triangles,” *J. Phys. Soc. Jpn.*, vol. 82, p. 083709, 2013. [Online]. Available: <https://journals.jps.jp/doi/abs/10.7566/JPSJ.82.083709>
- [13] I. Rousochatzakis, R. Moessner, and J. v. d. Brink, “Frustrated magnetism and resonating valence bond physics in two-dimensional kagome-like magnets,” *Phys. Rev. B*, vol. 88, no. 19, p. 195109, nov 2013. [Online]. Available: <http://dx.doi.org/10.1103/PhysRevB.88.195109>
- [14] O. Derzhko, J. Richter, O. Krupnitska, and T. Krokhnalskii, “The square-kagome quantum Heisenberg antiferromagnet at high magnetic fields: The localized-magnon paradigm and beyond,” *Low Temp. Phys.*, vol. 40, no. 6, pp. 513–520, 2014. [Online]. Available: <https://doi.org/10.1063/1.4881184>
- [15] A. Ralko and I. Rousochatzakis, “Resonating-valence-bond physics is not always governed by the shortest tunneling loops,” *Phys. Rev. Lett.*, vol. 115, p. 167202, Oct 2015. [Online]. Available: <https://link.aps.org/doi/10.1103/PhysRevLett.115.167202>
- [16] H. Nakano, Y. Hasegawa, and T. Sakai, “Magnetization jump in the magnetization process of the spin-1/2 Heisenberg antiferromagnet on a distorted square-kagome lattice,” *J. Phys. Soc. Jpn.*, vol. 84, no. 11, p. 114703, 2015. [Online]. Available: <https://doi.org/10.7566/JPSJ.84.114703>
- [17] O. Derzhko, J. Richter, and M. Maksymenko, “Strongly correlated flat-band systems: The route from heisenberg spins to hubbard electrons,” *Int. J. Mod. Phys. B*, vol. 29, no. 12, p. 1530007, 2015. [Online]. Available: <https://www.worldscientific.com/doi/abs/10.1142/S0217979215300078>
- [18] Y. Hasegawa, H. Nakano, and T. Sakai, “Metamagnetic jump in the spin- $\frac{1}{2}$ antiferromagnetic Heisenberg model on the square kagome lattice,” *Phys. Rev. B*, vol. 98, p. 014404, Jul 2018. [Online]. Available: <https://link.aps.org/doi/10.1103/PhysRevB.98.014404>
- [19] K. Morita and T. Tohyama, “Magnetic phase diagrams and magnetization plateaus of the spin-1/2 antiferromagnetic Heisenberg model on a square-kagome lattice with three nonequivalent exchange interactions,” *J. Phys. Soc. Jpn.*, vol. 87, no. 4, p. 043704, 2018. [Online]. Available: <https://doi.org/10.7566/JPSJ.87.043704>
- [20] T. Lukan, L. D. C. Jaubert, and A. Ralko, “Topological nematic spin liquid on the square kagome lattice,” *Phys. Rev. Research*, vol. 1, p. 033147, Dec 2019. [Online]. Available: <https://link.aps.org/doi/10.1103/PhysRevResearch.1.033147>
- [21] P. A. McClarty, M. Haque, A. Sen, and J. Richter, “Disorder-free localization and many-body quantum scars from magnetic frustration,” *Phys. Rev. B*, vol. 102, p. 224303, Dec 2020. [Online]. Available: <https://link.aps.org/doi/10.1103/PhysRevB.102.224303>
- [22] Y. Kuno, T. Mizoguchi, and Y. Hatsugai, “Flat band quantum scar,” *Phys. Rev. B*, vol. 102, p. 241115(R), Dec 2020. [Online]. Available: <https://link.aps.org/doi/10.1103/PhysRevB.102.241115>
- [23] N. Astrakhantsev, F. Ferrari, N. Niggemann, T. Müller, A. Chauhan, A. Kshetrimayum, P. Ghosh, N. Regnault, R. Thomale, J. Reuther, T. Neupert, and Y. Iqbal, “Pinwheel valence bond crystal ground state of the spin- $\frac{1}{2}$ Heisenberg antiferromagnet on the shuriken lattice,” *Phys. Rev. B*, vol. 104, p. L220408, Dec 2021. [Online]. Available: <https://link.aps.org/doi/10.1103/PhysRevB.104.L220408>
- [24] P. Schmoll, A. Kshetrimayum, J. Naumann, J. Eisert, and Y. Iqbal, “Tensor network study of the spin-1/2 Heisenberg antiferromagnet on the shuriken lattice,” 2022. [Online]. Available: <https://journals.aps.org/prb/abstract/10.1103/PhysRevB.107.064406>

- [25] J. Richter and J. Schnack, “Magnetism of the $s = \frac{1}{2}$ J_1 - J_2 square-kagome lattice antiferromagnet,” *Phys. Rev. B*, vol. 107, p. 245115, Jun 2023. [Online]. Available: <https://link.aps.org/doi/10.1103/PhysRevB.107.245115>
- [26] M. Gembé, H.-J. Schmidt, C. Hickey, J. Richter, Y. Iqbal, and S. Trebst, “Noncoplanar magnetic order in classical square-kagome antiferromagnets,” *Phys. Rev. Res.*, vol. 5, p. 043204, Jun 2023. [Online]. Available: <https://link.aps.org/doi/10.1103/PhysRevResearch.5.043204>
- [27] N. Niggemann, N. Astrakhantsev, A. Ralko, F. Ferrari, A. Maity, T. Müller, J. Richter, R. Thomale, T. Neupert, J. Reuther, Y. Iqbal, and H. O. Jeschke, “Quantum paramagnetism in the decorated square-kagome antiferromagnet $\text{Na}_6\text{Cu}_7\text{BiO}_4(\text{PO}_4)_4\text{Cl}_3$,” *Phys. Rev. B*, vol. 108, p. L241117, Dec 2023. [Online]. Available: <https://link.aps.org/doi/10.1103/PhysRevB.108.L241117>
- [28] M. Fujihala, K. Morita, R. Mole, S. Mitsuda, T. Tohyama, S.-i. Yano, D. Yu, S. Sota, T. Kuwai, A. Koda, H. Okabe, H. Lee, S. Itoh, T. Hawaii, T. Masuda, H. Sagayama, A. Matsuo, K. Kindo, S. Ohira-Kawamura, and K. Nakajima, “Gapless spin liquid in a square-kagome lattice antiferromagnet,” *Nat. Commun.*, vol. 11, p. 3429, 2020. [Online]. Available: <https://doi.org/10.1038/s41467-020-17235-z>
- [29] O. V. Yakubovich, L. V. Shvanskaya, G. V. Kiriukhina, A. S. Volkov, O. V. Dimitrova, and A. N. Vasiliev, “Hydrothermal synthesis and a composite crystal structure of $\text{Na}_6\text{Cu}_7\text{BiO}_4(\text{PO}_4)_4[\text{Cl}(\text{OH})_3]$ as a candidate for quantum spin liquid,” *Inorganic Chemistry*, vol. 60, no. 15, pp. 11 450–11 457, 2021. [Online]. Available: <https://doi.org/10.1021/acs.inorgchem.1c01459>
- [30] B. Liu, Z. Zeng, A. Xu, Y. Sun, O. Yakubovich, L. Shvanskaya, S. Li, and A. Vasiliev, “Low-temperature specific-heat studies on two square-kagome antiferromagnets,” *Phys. Rev. B*, vol. 105, p. 155153, Apr 2022. [Online]. Available: <https://link.aps.org/doi/10.1103/PhysRevB.105.155153>
- [31] M. Markina, P. Berdonosov, T. Vasilchikova, K. Zakharov, A. Murtazoev, V. Dolgikh, A. Moskvina, V. Glazkov, A. Smirnov, and A. Vasiliev, “Static and resonant properties of decorated square kagome lattice compound $\text{KCu}_7(\text{TeO}_4)(\text{SO}_4)_5\text{Cl}$,” 2022. [Online]. Available: <https://arxiv.org/abs/2212.11623>
- [32] A. F. Murtazoev, K. A. Lyssenko, M. M. Markina, V. A. Dolgikh, A. N. Vasiliev, and P. S. Berdonosov, “New Nabokoite-like Phases $\text{ACu}_7\text{TeO}_4(\text{SO}_4)_5\text{Cl}$ ($A = \text{Na}, \text{K}, \text{Rb}, \text{Cs}$) with Decorated and Distorted Square Kagome Lattices,” *ChemPhysChem*, vol. 24, p. e202300111, 2023. [Online]. Available: <https://chemistry-europe.onlinelibrary.wiley.com/doi/abs/10.1002/cphc.202300111>
- [33] D. Coffey and S. A. Trugman, “Magnetic properties of undoped C_{60} ,” *Phys. Rev. Lett.*, vol. 69, p. 176, 1992. [Online]. Available: <https://journals.aps.org/prl/abstract/10.1103/PhysRevLett.69.176>
- [34] C. Schröder, H.-J. Schmidt, J. Schnack, and M. Luban, “Metamagnetic phase transition of the antiferromagnetic Heisenberg icosahedron,” *Phys. Rev. Lett.*, vol. 94, p. 207203, 2005. [Online]. Available: <http://link.aps.org/abstract/PRL/v94/e207203>
- [35] N. P. Konstantinidis, “Antiferromagnetic Heisenberg model on clusters with icosahedral symmetry,” *Phys. Rev. B*, vol. 72, p. 064453, 2005. [Online]. Available: <http://link.aps.org/abstract/PRB/v72/e064453>
- [36] —, “Unconventional magnetic properties of the icosahedral symmetry antiferromagnetic Heisenberg model,” *Phys. Rev. B*, vol. 76, p. 104434, 2007. [Online]. Available: <http://link.aps.org/abstract/PRB/v76/e104434>
- [37] N. Konstantinidis, “Zero-temperature magnetic response of small fullerene molecules at the classical and full quantum limit,” *JMMM*, vol. 449, pp. 55–62, 2018. [Online]. Available: <https://www.sciencedirect.com/science/article/pii/S0304885317308235>
- [38] —, “Origin of the classical magnetization discontinuities of the dodecahedron,” 2023. [Online]. Available: <https://arxiv.org/pdf/2311.17205.pdf>
- [39] M. E. Zhitomirsky, M. V. Gvozdikova, and T. Ziman, “Noncoplanar multi-k states in frustrated spinel and kagome magnets,” *Ann. Phys.*, vol. 447, p. 169066, 2022. [Online]. Available: <https://doi.org/10.1016/j.aop.2022.169066>
- [40] H.-J. Schmidt and J. Richter, “Classical ground states of spin lattices,” *J. Phys. A: Math. Theor.*, vol. 55, no. 46, p. 465005, nov 2022. [Online]. Available: <https://dx.doi.org/10.1088/1751-8121/aca36d>
- [41] H.-J. Schmidt, “Theory of ground states for classical Heisenberg spin systems I,” 2017. [Online]. Available: <https://arxiv.org/abs/1701.02489v2>
- [42] —, “Theory of ground states for classical Heisenberg spin systems IV,” 2017. [Online]. Available: <https://arxiv.org/abs/1710.00318>